iScience

CellPress
OPEN ACCESS

Article

In situ tunable droplet adhesion on a super-repellent surface via electrostatic induction effect

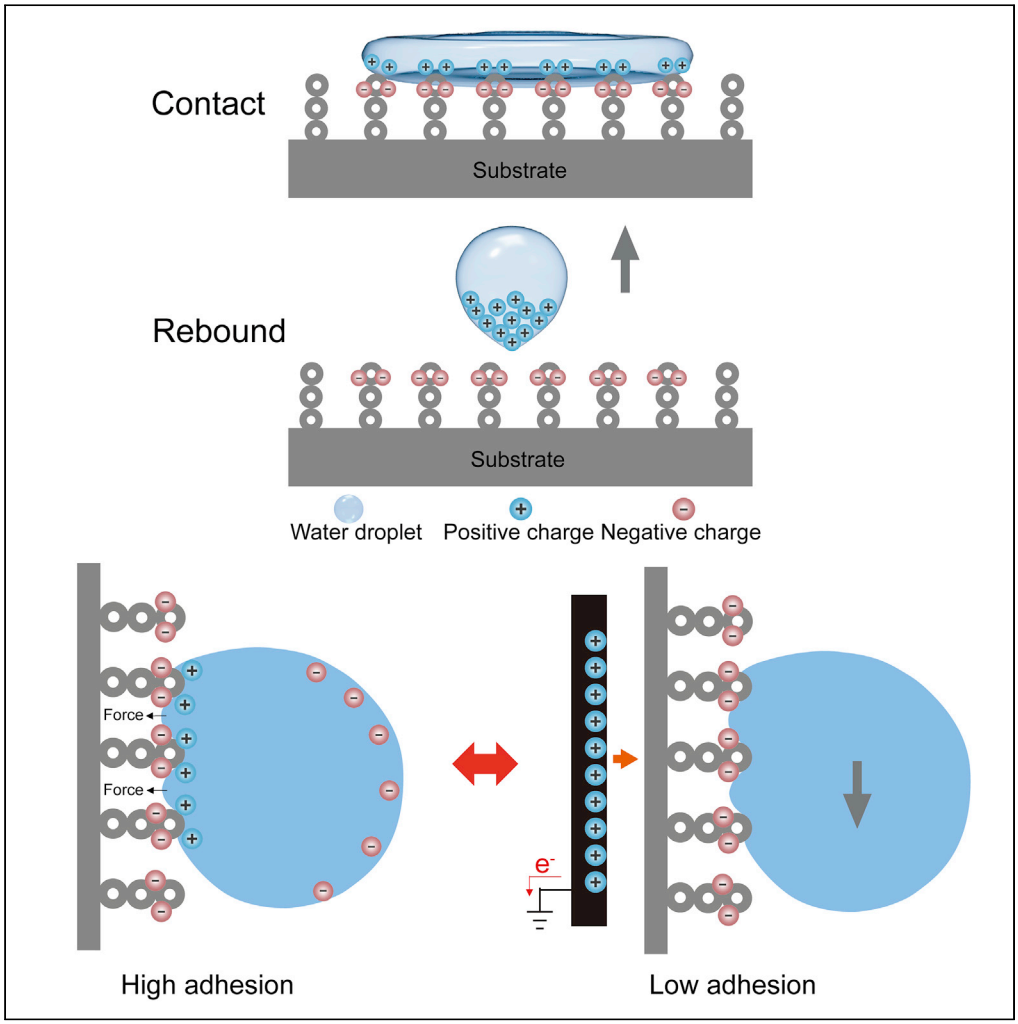

Qiangqiang Sun, Shiji Lin, Dehui Wang, Yong Li, Jinlong Yang, Xu Deng

wangdehui@uestc.edu.cn (D.W.)
liyong-ccsi@uestc.edu.cn (Y.L.)
jinlongy@uestc.edu.cn (J.Y.)

HIGHLIGHTS

Substrate-dependent surface adhesion after droplet impact is systematically studied

Reversibly tunable surface adhesion with high magnitude is achieved

Efficient droplet sorting and manipulation are demonstrated

Sun et al., iScience *24*, 102208
March 19, 2021
https://doi.org/10.1016/j.isci.2021.102208

iScience

CellPress
OPEN ACCESS

Article

In situ tunable droplet adhesion on a super-repellent surface via electrostatic induction effect

Qiangqiang Sun,[1,2] Shiji Lin,[3] Dehui Wang,[1,*] Yong Li,[1,*] Jinlong Yang,[1,4,*] and Xu Deng[1]

SUMMARY

In this paper, we report a finding that substrate affects the adhesion of charged super-repellent surfaces. Water droplet impacting on a super-repellent surface produces surface charge, whose expression depends on the substrate. The charged super-repellent surface is sticky to droplets for a suspended substrate made of dielectric materials, while it has low adhesion for a conducting substrate or stage attached at the bottom because of electrostatic induction. Theoretical analysis and simulation are conducted to elucidate the mechanism of substrate effect on surface adhesion. Finally, we develop a new approach to reversibly tune the adhesion of super-repellent surface by combining surface-charge-induced adhesion increase and electrostatic-induction-regulated express of net surface charge. As a proof-of-concept experiment, we demonstrate that droplet sorting and manipulations can be realized by using this controllable surface adhesion tuning approach, which has potential applications in advanced lab-on-a-drop platform.

INTRODUCTION

Smart surfaces with specific liquid-solid interfacial adhesion are crucial in a variety of applications, including lab-on-chip devices (Milionis et al., 2014), biochemical analysis (Sun and Qing, 2011), cell adhesion (Didar and Tabrizian, 2010; Ishizaki et al., 2010), and no loss droplet transportation (Dai et al., 2019; Ding et al., 2012; Li et al., 2011; Tang et al., 2017; Wu et al., 2011; Yang et al., 2018). Different applications require specific liquid-solid interfacial adhesion for controllable droplet mobility on the surface. Typically, a low adhesion surface shows great advantages in applications due to their excellent anti-fouling properties. In some applications, certain surface adhesion is desired for a specific usage (Callies and Quéré, 2005; Deng et al., 2012; Miwa et al., 2000; Tuteja et al., 2007).

Intensive research studies have focused on designing surface morphology and chemical composite for tuning adhesion to water droplet. The specific adhesive surface is prepared by controlling various parameters. For example, morphologies, like nanopore arrays, nanotube arrays, and nanovesuvianite structures, produce different adhesive forces (Lai et al., 2009). The orientations of surface microstructures are also designed to tune the liquid-solid interface adhesion on the same super-repellent surface (Zheng et al., 2007). Chemical composite of the surface molecule is an alternative way to obtain high adhesion super-repellent surface. Examples include adhesion adjustment of TiO_2 films using 1*H*, 1*H*, 2*H*, 2*H*-perfluorooctyltriethoxysilane, and nitrocellulose (Lai et al., 2008) or adjustable adhesion achieved by boiling coating (Ding et al., 2018). Although these strategies are effective for preparing the super-repellent surface with low or high water adhesion, the process is irreversible, and therefore, the wettability of the surface is constant after treatment. In practical applications, active control of the adhesion is desired.

To adaptively control the adhesion of surfaces, low surface energy materials were commonly used while external stimuli were employed for the adjustment. Strategies, including heat, light, pH, magnetic field, and electric field, have been used in the reversible regulation of adhesion. However, problems like complexity in setup, slow response, external energy consumption, additive to the sample droplets, and small tuning amplitude are unavoidable in these methods (Cheng et al., 2008; Heng et al., 2015; Li et al., 2009). Simple, real-time control methods for reversible adjustment with a wide range of surface adhesion still present a challenge.

[1]Center for Materials Surface Science, Institute of Fundamental and Frontier Sciences, University of Electronic Science and Technology of China, Chengdu 610054, P. R. China

[2]Key Laboratory of Advanced Technologies of Materials, Ministry of Education, School of Materials Science and Engineering, Southwest Jiaotong University, Chengdu 610031, P. R. China

[3]School of Physics, University of Electronic Science and Technology of China, Chengdu 610054, P. R. China

[4]Lead contact

*Correspondence: wangdehui@uestc.edu.cn (D.W.), liyong-ccsi@uestc.edu.cn (Y.L.), jinlongy@uestc.edu.cn (J.Y.)

https://doi.org/10.1016/j.isci.2021.102208

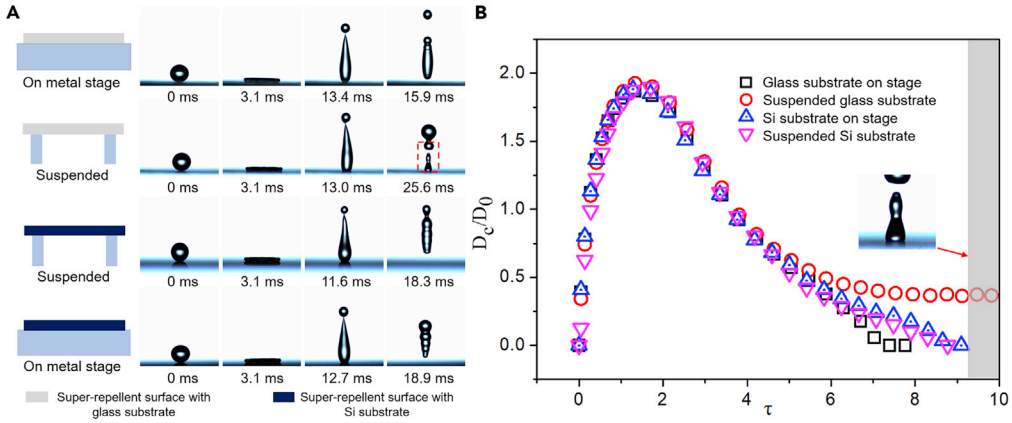

Figure 1. The spread and retraction process of droplet impact on super-repellent surfaces

(A) Snapshots of water droplet impact on the super-repellent surface with glass substrate placed on a metal stage (upper panel), suspended in air (second panel), the super-repellent surface with suspended Si substrate (third panel), and Si substrate on a metal stage (bottom panel), respectively (*We* = 34).

(B) Time-resolved variations of droplet contact length D_c normalized by the droplet diameter D_0 on the surface in the spreading and retracting process.

We have reported that the surface charge can be created by water impact on a super-repellent surface coated on a piece of thin glass substrate (Sun et al., 2019). Using this intense yet highly localized electric field on the top of the surface, we are able to create strong adhesion of the drop on the surface. Here, we investigated the expression of the electric field, which could be influenced by the substrate. Although all surfaces are supported by a substrate, consideration of the effect of the substrate on the surface property was usually neglected. We investigate the adhesion of a charged super-repellent surface regulated by the substrate. The surface adhesive force to droplets is disparate at the charged position when the substrate is different. Based on this finding, we develop an in situ strategy to adjust the surface adhesion reversibly and realize the droplet manipulation by actively controlling a conductive substrate.

RESULTS AND DISCUSSION

Increase in surface adhesion after drop impact on super-repellent surfaces with different types of substrates

When a drop impacted on the prepared super-repellent surface, we found that the retraction process was strikingly distinct when the type of placing or substrate was changed. To demonstrate the difference in drop impacting process, we prepared two sample surfaces with the same super-repellent coating on varied substrates (Figure 1A). When a droplet impacted on a super-repellent surface with a thin glass substrate placed on a metal stage, the droplet rebounded and detached completely. On the other hand, a droplet split to a small droplet adhering on the impacted position under the same condition, except that the surface was suspended in the air. If the substrate was replaced by a silicon wafer, which is either suspended or placed on a metal substrate, such adhesion effect was remarkably mitigated. It can be found that the adhesion difference of super-repellent surface could be tuned by the substrate property and platform. The whole process is shown in Figure 1B, demonstrated by the ratio of contact diameter (D_c) and the diameter of the droplet (D_0) as a function of normalized time ($\tau = \sqrt{\sigma t^2/\rho r_0^3}$). Here, σ is the surface tension of water, t is the time from contact, ρ is the density of the water, and r_0 is the radius of the droplet. The curves demonstrate that the spreading processes are identical but the rebounding process is hindered on the suspended super-repellent surface with a thin glass substrate. The droplet rebound test also indicates that the substrate of the impacted super-repellent surface heavily affects the surface adhesion (Figure S1). A droplet was released from 1 cm height onto the super-repellent surface which was previously impacted by water droplets with different Weber numbers ($We=\rho v^2 r_0/\sigma$). Here, v is the impact velocity. Droplet on the suspended glass one always stops earliest because of the increased surface adhesion.

To verify the influence of the substrate on adhesion, we further measured the adhesive force at the position on the surface after water drop impacting. The measurement process is shown in Figure 2A. The super-repellent surface approaches to, contacts, and then retracts from a hanging water drop. Figure 2B

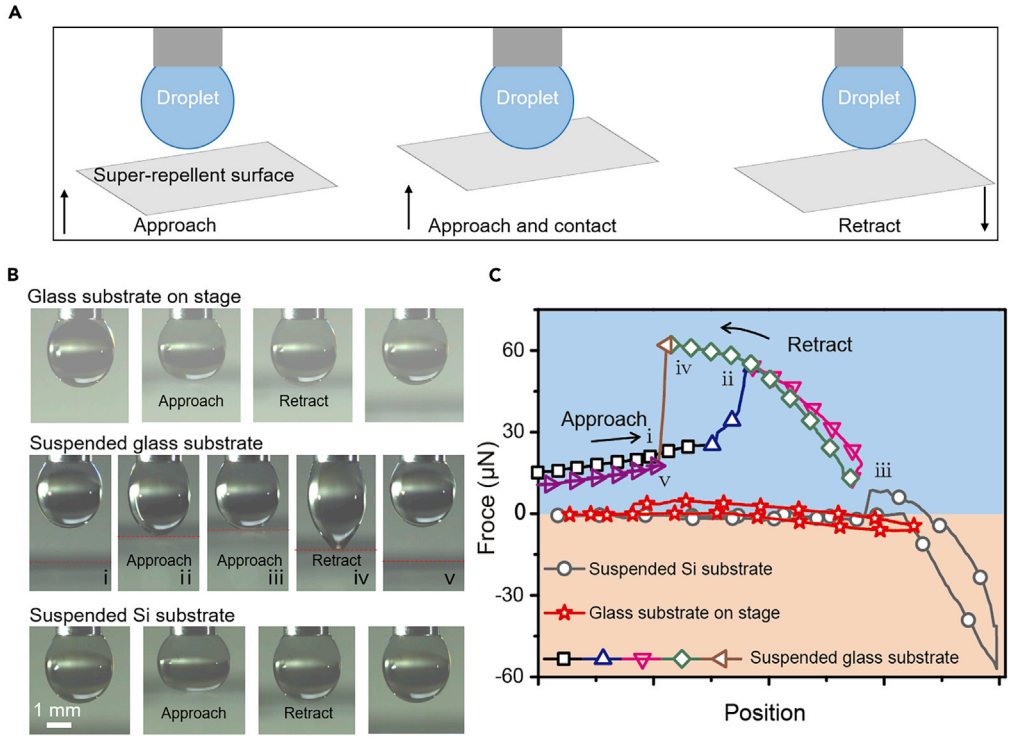

Figure 2. Adhesion test of super-repellent surface

(A) Schematics showing the process of a super-repellent surface approaching to and retracting from a hanged water drop in the adhesion test.

(B) Snapshots of droplet interaction with impacted glass-substrate super-repellent surface placed on a stage (upper panel) and suspended in air (**i**-**v**). The bottom panel is the Si-substrate super-repellent surface (*We* = 47.6).

(C) Force-distance curves during the impacted super-repellent surface approaching to and retracting from a hanged droplet corresponding to (A).

shows the shapes of the water droplet during the adhesive force measurement. The droplet has obvious elongation on the suspended surface fabricated with the thin glass substrate, compared with the other two surfaces. To clarify the procedure of the measurement, the approaching and detaching steps were denoted as i-v, respectively. Image **i** in Figure 2B is obtained before the surface contacts with the water droplet. At this stage, no obvious deformation was noticed because of the large distance between the drop and the surface. When the droplet further approached the surface, the water droplet was attracted onto the suspended surface prepared with the thin glass substrate (image ii), while this process was not found in the other two samples. The obvious elongation on the drop indicates that an attraction force exerts on the droplet. Image **iii** shows the snapshot when the surface keeps closing the droplet. The deformation of the droplet was mitigated with the increasing height of the stage. Image **iv** is the moment before the separation between surface and droplet, which represents the magnitude of the surface's adhesion. Large deformation was observed on the thin suspended glass substrate, compared to the other two samples. Image **v** is the droplet after detaching from the surface. From these images, it is apparent that the substrate has a significant influence on the adhesive force of the impacted super-repellent surface. The details of force measured in this process are plotted in Figure 2C. The adhesive force of the drop-impacted suspended super-repellent surface on the thin glass is nearly six-fold larger than that on the other two surfaces. Contact angle and roll-off angle measurement (Table S1) also indicates an obvious increase in adhesion for the suspended super-repellent surface on the thin glass.

We analyze that the increased adhesion comes from the surface charge generated from water droplet contacting and separating. It has been demonstrated that the super-repellent surface was charged when a water droplet impacted the surface (Sun et al., 2019). A droplet sitting on the charged super-repellent surface could be attracted by dielectrophoresis force, originated from the non-uniform electric field generated by

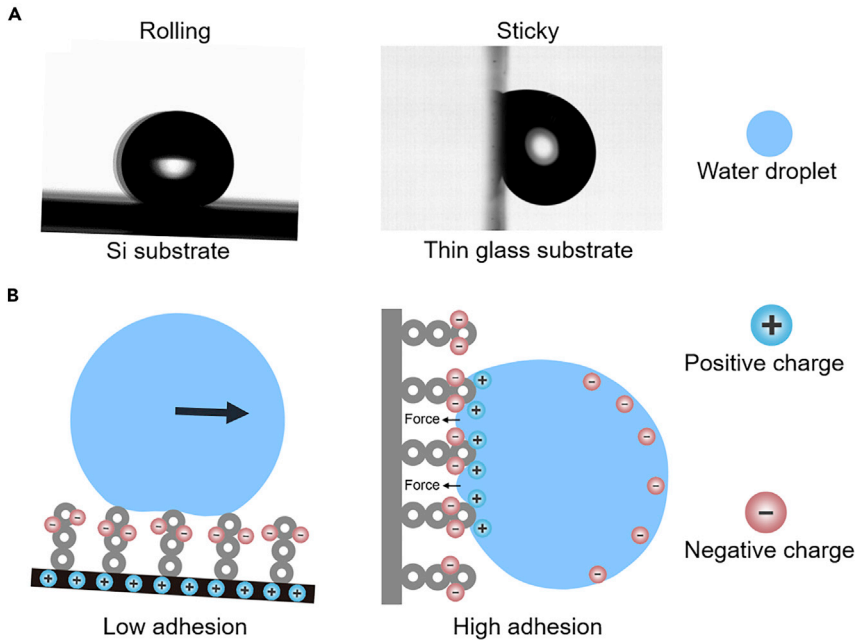

Figure 3. The effect of substrate on surface-droplet adhesion

(A) Droplet states on charged super-repellent surface by impact of an 8 μL of water drop (*We* = 47.6).

(B) Schematics of the substrate's effect on surface adhesion through electrostatic induction.

the charged surface. The adhesive force for a water droplet (considering a spherical particle) with radius r_0 can be calculated by the following equation (Pethig, 2010):

$$F_{adh} \approx F_{DEP} = 2\pi {r_0}^3 \varepsilon_r' \varepsilon_0 \frac{\varepsilon_r' - 1}{\varepsilon_r' + 2} \nabla {E_{net}}^2 \qquad \text{(Equation 1)}$$

where E_{net} is electric field strength, ε_r' is the relative dielectric constant of water, and ε_0 is the vacuum dielectric constant. For a water droplet with a certain radius, the adhesive force depends on the distribution of electric field. Though the charge distribution on the super-repellent coating is identical after droplet impacting at the same condition, the expression of the charge, namely the electric field, is largely influenced by the substrate underneath the coating.

The effect of substrate on surface adhesion

To demonstrate the effect of the substrate on the surface adhesive force, we measured the roll-off angle of the droplet located on the charged surface. The droplet on the charged super-repellent surface fabricated with a Si substrate or placed on a metal stage easily rolls down because of the meager adhesive force. The suspended charged super-repellent surface with a thin glass substrate is very sticky to the droplet (Figure 3A). In order to clarify how substrate and stage influence the surface adhesion, we consider the effect of substrate and stage on surface charge expression. We have analyzed that the substrate polarization can reduce the net surface charge (Q_{net}) on the super-repellent surface (Sun et al., 2019). The substrate effect is presented in Figure 3B. Surface charge generates and exists on super-repellent coating after droplet impacting. The substrate produces an opposite positive charge to reduce the net surface charge through electrostatic induction. The net charge after induction can be expressed as follows (Sun et al., 2019):

$$Q_{net} = Q - \Delta Q_{pol} = Q - \left(\varepsilon_r^s - 1\right)\varepsilon_0 A \int_0^L \nabla \cdot E dL \qquad \text{(Equation 2)}$$

where Q is the original surface charge, ε_r^s is the relative dielectric constant of the substrate material, A is the cross-sectional area of polarization, E is the electric field due to the surface charge, and L is the thickness of the substrate. It is concluded that the net or effective surface charge depends on the dielectric constant and the thickness of the substrate. For a suspended thin glass substrate, the expression of surface charge is barely influenced because of the low dielectric constant and thickness. On the other hand, because of the large dielectric constant for Si substrate and the infinite dielectric constant and thickness of the metal

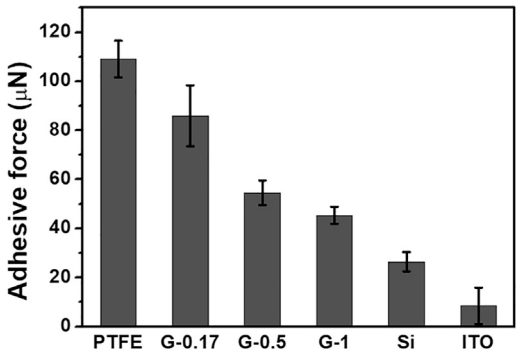

Figure 4. The adhesive force of charged super-repellent surface fabricated with different substrates (*We* = 68.1)

stage, the charge on super-repellent surface fabricated with Si substrate or placed on a metal stage is almost completely screened so as not to express, resulting in a low adhesion. A similar result is reported on solid-solid contact electrification. The distant substrates influence the outcome of contact electrification because the image charges induced in conductive supports can feedback the original surface charges (Siek et al., 2018). Since the surface adhesion is determined by the net surface charge according to Equation 1, the substrate's dielectric property and thickness can be used to control the adhesion of the super-repellent surface.

We have verified the substrate effect on adhesion of the charged super-repellent surface, using materials with various dielectric constant and thickness as the substrate of super-repellent surfaces. All surfaces are charged by the mean of water drop impact at the same condition. As shown in Figure 4, the adhesive force of the charged surface decreases with the increase of the substrate's dielectric constant and thickness. The material properties are listed in Table S2. The experiment result fits well with our theoretical analysis above.

Reversibly tunable surface adhesion

According to the basic principle of substrate effect on the expression of charged super-repellent surface, we are able to tailor the surface adhesion precisely and reversibly through a removable conductive substrate. To demonstrate the tunable adhesion on a charged surface, we moved a copper plate to the surface to influence the expression of the charge. A droplet is stick onto the charged position on a super-repellent surface made from a thin glass slide and will not roll off even the surface was placed vertically. When a copper plate approaches the backside of the impacted position on the super-repellent surface, the droplet rolls off because of electrostatic induction between the copper plate and surface charge (Figure 5A). This process is analyzed based on the model mentioned above. The conductive plate reduces the net surface charge, which causes adhesion reduction. The electrostatic induction process reduces the surface charge density due to the image charge on metal, and the induction distance (D) determines the reduction amount of surface charge (Figure 5A and Video S1). The schematics illustrate the electrostatic induction process in Figure 5B. The positive charge generates at the side close to the negative surface charge and partly cancels the net charge. At the same time, the opposite charge forms at the far end of the conductor or bleed off to the ground. The distance between the metal plate and super-repellent surface determines the electrostatic induction intensity. Closer induction distance leads to less net charge.

We analyze this process by simplifying the surface charge to point charge because the charged area is small. The electric field intensity (E) produced by the original surface charge Q at one point in metal is $E = \frac{Q}{4\pi\varepsilon_0(D+d)^2}$, where d is the distance between the point to the metal surface which is a constant. The tiny thickness and dielectric constant of the super-repellent surface are negligible. When a metal plate is moved close to the charged surface, the electric field across the metal drives the motion of charge to produce an equivalent and heterogeneous electric field to balance the former. As a result of electrostatic induction, the opposite charge (q) generated on the metal surface is $q = -\frac{Qd^2}{(D+d)^2}$. The net charge after induction is expressed as follows:

$$Q_{Net} = Q + q = Q - \frac{Qd^2}{(D+d)^2} \qquad \text{(Equation 3)}$$

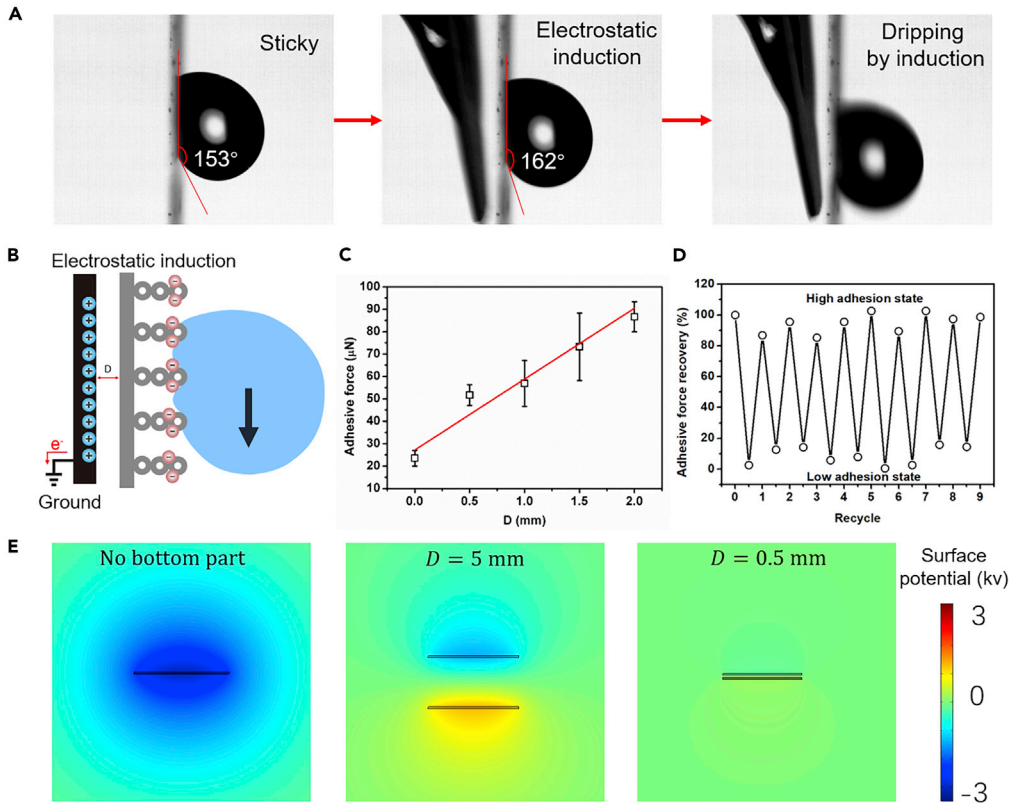

Figure 5. Electrostatic induction regulated surface-droplet adhesion

(A) Snapshots of droplet rolling off when a copper plate closes to the surface.

(B) Schematics of electrostatic induction between a conductor and surface charge to induce adhesion change.

(C) Controllable adhesive force of the charged surface (*We* = 40.8) through electrostatic induction at different distances.

(D) The switch of high and low adhesion state through substrate effect.

(E) Simulation of substrate effect on surface charge expression.

Thus, we can control the net surface charge by adjusting *D*. The electric field strength around the super-repellent surface depends on the net surface charge density, allowing us to tune the surface adhesion. The roll-off angle changing trend with *D* confirms this (Figure S2). Figure 5B shows that the adhesive force control from 20 μN to 90 μN is achieved by changing the induction distance. The lower limit of the adhesion (~20 μN) is larger than that on the pristine candle-soot-templated super-repellent surface. This is caused by the residue electric field after induction. In this way, the adhesion of charged super-repellent surface is reversible between high adhesion state and low adhesion state (Figure 5D). We also confirmed that other types of super-repellent surfaces can be used to regulate the adhesion. We have fabricated another two super-repellent surfaces by commercial spray coating of Ultra-Ever Dry and Glaco on 170-μm-thick glass substrates. The adhesion of these surfaces can still be enhanced in the same way of droplet impact (Figure S3). The differences in the value of elevated adhesion among these superhydrophobic surfaces under the same impact dynamics are probably caused by the structure or roughness of the prepared surfaces. Since the charging process is rewritable and programmable (Sun et al., 2019), we can even design the adhesion at the appointed position in a programmable way by controlling the water impact and electrostatic induction parameters. It should be noted that the maximum reversible adhesion was determined by the surface charge density. This is essentially different from the traditional electrowetting on the super-repellent surface. The magnitude of the adhesion in these techniques is mostly limited by the breakup of the Cassie-Baxter state (Yang et al., 2019). The maximum adhesion reported here was attributed to the dense charge distributed on top of the super-repellent coating (Figures 3B and 5B).

To further demonstrate the influence of the movable conductive substrate on surface charge expression, we simulated the electric potential distribution around the charged surface with varied induction distances using COMSOL software. The parameters used in this simulation are listed in Table S3. As shown in

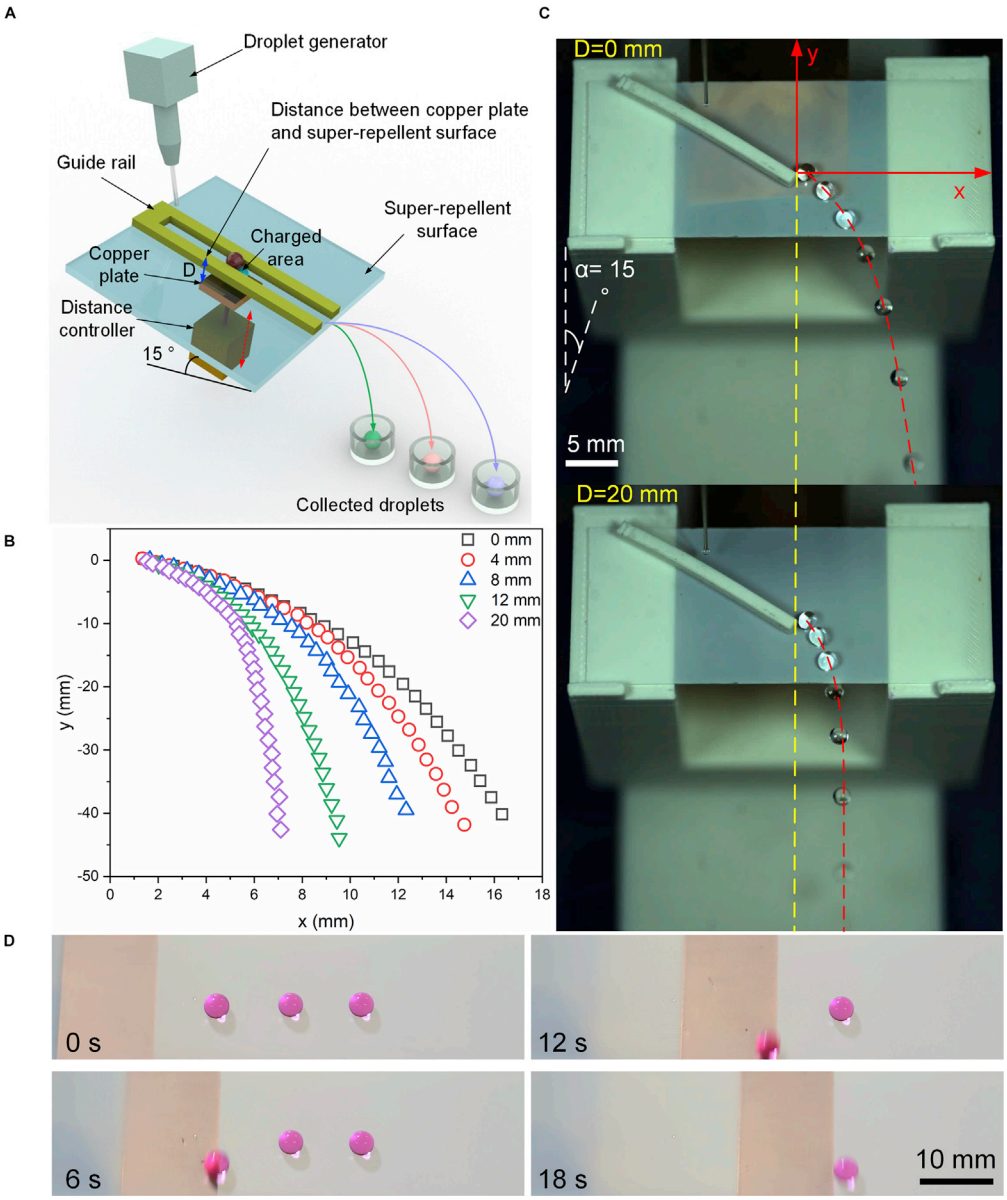

Figure 6. Droplet sorting and manipulation

(A) Schematic of droplet sorting process based on tunable surface adhesion. The device is titled at 15°. *D* presents the electrostatic induction distance.

(B) Droplet-advancing distance as a function of electrostatic induction distance.

(C) Time-lapsed images of droplet advancing at different electrostatic induction distances. *D* presents the electrostatic induction distance.

(D) Droplet trap and release. The super-repellent surface on a thin glass substrate becomes adhesive to seize droplet after impact (*We* = 34.0) and returns to low adhesion via electrostatic induction (*D* = 0.5 mm). The surface is titled at an angle of 20°.

Figure 5E, the actual electric field strength around the charged surface reduces as the conductive plate closes to the surface. The weakened electric field causes the reduction of surface adhesive force.

Demonstration of droplet sorting and manipulation by tunable surface adhesion

We demonstrate the potential application of tunable droplet adhesion on the super-repellent surface via electrostatic induction effect for droplet sorting, as sketched in Figure 6A. Droplets are released to a

super-repellent surface with a tilted angle of 15°. A baffle is used for guiding the droplet rolling path that the droplet travels across the charged area. A copper plate as a conductor is movable for adjusting the electrostatic induction distance. When we set different values for the induction distance (0–20 mm), the droplets rolling length is distinguished so as to realize droplet sorting (Figure 6B). The time-lapsed images of the sorting process on this super-repellent surface with tunable adhesion show the capacity of this device to separate droplets (Figure 6C). With the strongest electrostatic induction effect at the distance of 0 mm, the drop advanced at a certain distance and finally fell off the surface. In contrast, the advancing distance of the drop significantly decreased at the electrostatic induction distance of 20 mm, and the drop fell off the surface at a shorter distance. This device runs without requiring electric power and an electrode, which is beneficial for extensive applications. Moreover, we have demonstrated another application for selectively trapping and releasing droplets. As shown in Figures 6D and Video S2, the charged position on the super-repellent surface serves as the trapping positions of a three-water-droplet array with the help of high adhesion. Using a piece of metal approaching to the droplet underneath the substrate, the trapped droplets can be released in a programmable way under the effect of electrostatic induction. This droplet trap and release approach is useful in biomedical and bioanalysis process.

Conclusion

In conclusion, we found the charged super-repellent surface with a thin dielectric substrate is highly adhesive when it is suspended. On the other hand, the charged surface with a conductive substrate or placed on a metal stage behaves low adhesion. We analyzed the substrate effect on impacted surface adhesion based on surface charge and electrostatic induction. Further, we introduced a movable conductor to tune the adhesion of the impacted super-repellent surface. The distance between the conductive plate and the charged surface determines the amount of adhesive force on the basis of the theoretical analysis and electric simulation. Combining the dielectric substrate with a movable conductive plate, the adhesive force of the super-repellent surface can be easily regulated after charging by droplet impact. Droplet manipulation is demonstrated based on this adjustment method for surface adhesion. From a broader perspective, the reversible adhesion change illustrates that the surface charge does not dissipate but always exists at the position after water contact even when the substrate is a conductor or is placed on a stage. It is noteworthy that the charge on the super-repellent surface may have an imperceptible effect on the wetting experiment besides adhesion.

Limitations of the study

The increased surface adhesion comes from the generated surface charge, whose stability is influenced by the environmental humidity. We need to recharge the super-repellent surface if the charge decays, especially in high air humidity conditions. The adhesion can be tuned to extremely low when there is no surface charge or the charge is screened, but the surface charge density has an upper limit, leading to the surface adhesion cannot be infinite.

RESOURCE AVAILABILITY

Lead contact

Further information and requests for resources and materials should be directed to and will be fulfilled by the lead contact, Jinlong Yang (jinlongy@uestc.edu.cn).

Materials availability

This study did not generate new unique reagents.

Data and code availability

This study did not produce datasets/code.

METHODS

All methods can be found in the accompanying transparent methods supplemental file.

SUPPLEMENTAL INFORMATION

Supplemental information can be found online at https://doi.org/10.1016/j.isci.2021.102208.

ACKNOWLEDGMENTS

We acknowledge funding support by the National Natural Science Foundation of China (22072014), Fundamental Research Funds for the Central Universities (ZYGX2019J119), Max-Planck-Gesellschaft (Max Plank Partner Group UESTC-MPIP) and the Opening Project of State Key Laboratory of Polymer Materials Engineering (Sichuan University) (Grant No. sklpme2020-4-02), Sichuan Outstanding Young Scholars Foundation (2021JDJQ0013), and Sichuan Science and Technology Innovation Talents (2021JDRC0016).

AUTHOR CONTRIBUTIONS

Q.S., J.Y., and X.D designed and conceived the concept. Q.S. and Y.L. performed the experiments. S.L. simulated the electric field distribution. Q.S., Y.L., J.Y., D.W., and X.D. discussed the experimental data and wrote the manuscripts. X.D. supervised the work.

DECLARATION OF INTERESTS

The authors declare no competing interests.

Received: November 30, 2020
Revised: January 17, 2021
Accepted: February 16, 2021
Published: March 19, 2021

REFERENCES

Callies, M., and Quéré, D. (2005). On water repellency. Soft Matter *1*, 55–61.

Cheng, Z., Feng, L., and Jiang, L. (2008). Tunable adhesive superhydrophobic surfaces for superparamagnetic microdroplets. Adv. Funct. Mater. *18*, 3219–3225.

Dai, H., Gao, C., Sun, J., Li, C., Li, N., Wu, L., Dong, Z., and Jiang, L. (2019). Controllable high-speed electrostatic manipulation of water droplets on a superhydrophobic surface. Adv. Mater. *31*, 1905449.

Deng, X., Mammen, L., Butt, H.-J., and Vollmer, D. (2012). Candle soot as a template for a transparent robust superamphiphobic coating. Science *335*, 67–70.

Didar, T.F., and Tabrizian, M. (2010). Adhesion based detection, sorting and enrichment of cells in microfluidic Lab-on-Chip devices. Lab Chip *10*, 3043–3053.

Ding, C., Zhu, Y., Liu, M., Feng, L., Wan, M., and Jiang, L. (2012). PANI nanowire film with underwater superoleophobicity and potential-modulated tunable adhesion for no loss oil droplet transport. Soft Matter *8*, 9064–9068.

Ding, G., Jiao, W., Chen, L., Yan, M., Hao, L., and Wang, R. (2018). A self-sensing, superhydrophobic, heterogeneous graphene network with controllable adhesion behavior. J. Mater. Chem. A *6*, 16992–17000.

Heng, L., Guo, T., Wang, B., Fan, L.-Z., and Jiang, L. (2015). In situ electric-driven reversible switching of water-droplet adhesion on a superhydrophobic surface. J. Mater. Chem. A *3*, 23699–23706.

Ishizaki, T., Saito, N., and Takai, O. (2010). Correlation of cell adhesive behaviors on superhydrophobic, superhydrophilic, and micropatterned superhydrophobic/superhydrophilic surfaces to their surface chemistry. Langmuir *26*, 8147–8154.

Lai, Y., Gao, X., Zhuang, H., Huang, J., Lin, C., and Jiang, L. (2009). Designing superhydrophobic porous nanostructures with tunable water adhesion. Adv. Mater. *21*, 3799–3803.

Lai, Y., Lin, C., Huang, J., Zhuang, H., Sun, L., and Nguyen, T. (2008). Markedly controllable adhesion of superhydrophobic spongelike nanostructure TiO2 films. Langmuir *24*, 3867–3873.

Li, C., Guo, R., Jiang, X., Hu, S., Li, L., Cao, X., Yang, H., Song, Y., Ma, Y., and Jiang, L. (2009). Reversible switching of water-droplet mobility on a superhydrophobic surface based on a phase transition of a side-chain liquid-crystal polymer. Adv. Mater. *21*, 4254–4258.

Li, J., Liu, X., Ye, Y., Zhou, H., and Chen, J. (2011). Gecko-inspired synthesis of superhydrophobic ZnO surfaces with high water adhesion. Colloids Surf. A Physicochemical Eng. Aspects *384*, 109–114.

Milionis, A., Fragouli, D., Martiradonna, L., Anyfantis, G.C., Cozzoli, P.D., Bayer, I.S., and Athanassiou, A. (2014). Spatially controlled surface energy traps on superhydrophobic surfaces. ACS Appl. Mater. Interfaces *6*, 1036–1043.

Miwa, M., Nakajima, A., Fujishima, A., Hashimoto, K., and Watanabe, T. (2000). Effects of the surface roughness on sliding angles of water droplets on superhydrophobic surfaces. Langmuir *16*, 5754–5760.

Pethig, R. (2010). Dielectrophoresis: status of the theory, technology, and applications. Biomicrofluidics *4*, 022811.

Siek, M., Adamkiewicz, W., Sobolev, Y.I., and Grzybowski, B.A. (2018). The influence of distant substrates on the outcome of contact electrification. Angew. Chem. *130*, 15605–15609.

Sun, Q., Wang, D., Li, Y., Zhang, J., Ye, S., Cui, J., Chen, L., Wang, Z., Butt, H.-J., and Vollmer, D. (2019). Surface charge printing for programmed droplet transport. Nat. Mater. *18*, 936–941.

Sun, T., and Qing, G. (2011). Biomimetic smart interface materials for biological applications. Adv. Mater. *23*, H57–H77.

Tang, X., Zhu, P., Tian, Y., Zhou, X., Kong, T., and Wang, L. (2017). Mechano-regulated surface for manipulating liquid droplets. Nat. Commun. *8*, 14831.

Tuteja, A., Choi, W., Ma, M., Mabry, J.M., Mazzella, S.A., Rutledge, G.C., McKinley, G.H., and Cohen, R.E. (2007). Designing superoleophobic surfaces. Science *318*, 1618–1622.

Wu, D., Wu, S.Z., Chen, Q.D., Zhang, Y.L., Yao, J., Yao, X., Niu, L.G., Wang, J.N., Jiang, L., and Sun, H.B. (2011). Curvature-driven reversible in situ switching between pinned and roll-down superhydrophobic states for water droplet transportation. Adv. Mater. *23*, 545–549.

Yang, J., Wang, D., Liu, H., Li, L., Chen, L., Jiang, H.-R., and Deng, X. (2019). An electric-field-dependent drop selector. Lab Chip *19*, 1296–1304.

Yang, C., Wu, L., and Li, G. (2018). Magnetically responsive superhydrophobic surface: in situ reversible switching of water droplet wettability and adhesion for droplet manipulation. ACS Appl. Mater. Interfaces *10*, 20150–20158.

Zheng, Y., Gao, X., and Jiang, L. (2007). Directional adhesion of superhydrophobic butterfly wings. Soft Matter *3*, 178–182.

iScience, Volume *24*

Supplemental information

In situ tunable droplet adhesion on a super-repellent surface via electrostatic induction effect

Qiangqiang Sun, Shiji Lin, Dehui Wang, Yong Li, Jinlong Yang, and Xu Deng

Transparent Methods

Preparing super-repellent surface: Si wafer (ε_r = 12.1), ITO (ε_r = ∞) coated glass and glass slide (ε_r = 5.75) with various thicknesses (Deckglaser™ glass cover-slips), as substrates, were first coated with candle soot, then placed in a desiccator together with 1 ml of TEOS and 1 ml of ammonia solution. The desiccator was closed, and the vacuum was maintained for 20 h. Then, the carbon soot core was removed through annealing at 550 °C for 3 h in air. The annealed samples were treated with air plasma for 5 min using a Harrick plasma cleaner (Harrick Plasma, Ithaca, NY) at high power followed by another chemical vapor deposition sequence of 1H,1H,2H,2H-perfluorooctyltrichlorosilane (PFOTS, 0.1 ml) in vacuum for 2 h to lower the surface energy (Deng et al., 2012). Thus, a super-repellent surface with porous structure is obtained (Figure S4). Another substrate with PTFE plate (ε_r = 1.55) was coated by the commercial super-repellent coating Ultra-Ever Dry (Song et al., 2015). Glaco as a kind of commercial super-repellent coating is also used.

Adhesive force measurement: An 8 μl droplet of deionized water was dripped onto superamphiphobic surface from different heights (1-10 cm). The attraction force between the surface and water droplet was quantified using a high-sensitivity microelectromechanical balance system (Krüss K100 Tensiometer, Germany). A 15 μl water droplet was suspended on a metal needle, and a superamphiphobic surface that was approached and retracted from the suspended droplet at 4 mm/min. The force between the superamphiphobic surface and the water droplet was recorded during approach and retraction. At the same time, the motion of droplet was captured by a high-speed camera (Photron FASTCAM SA-5) at a rate of 1,000 fps. The relative humidity maintained at approximately 40%, and the room temperature was 25 °C.

Droplet impact test: Two kinds of surfaces, including the prepared super-repellent coating on 170 μm-thick glass and on Si substrate, were used in this experiment. An 8 μl of water droplet was released from a needle at the height of 5 cm onto the super-repellent surface. The substrates were either on a metal lifting platform or suspended in air by a holder contacting the two ends of the surface. A high-speed camera (Photron FASTCAM SA-5) recorded the impact processes at a rate of 7,000 fps. In the rebounding test, the surface was horizontally placed for recording. For adhesive measurement and applications, the droplet-impact-charging process was conducted on a tilted surface, where only single rebound of each impact was used.

Electric potential distribution simulation: The electric potential distribution induced by charged surfaces is modeled using COMSOL Multiphysics V5.3a. The electrostatic system is simplified to a two-dimensional problem with a computational domain of $40\ \mathrm{mm} \times 40\ \mathrm{mm}$ surrounding the surfaces. The surfaces are set as two parallel thin blocks with width w and length l equal to $10\ \mathrm{mm}$ and $0.17\ \mathrm{mm}$, respectively. The distance d between the two surfaces is varied (Figure S5).

The electric potential V is governed by the Poisson's equation:

$$\vec{\nabla} \cdot \vec{\nabla} V = -\frac{\rho_s}{\varepsilon_0} \tag{1}$$

where ρ_s is the surface charge density which is set as $-8 \times 10^{-6}\ \mathrm{C/m^2}$ and $8 \times 10^{-6}\ \mathrm{C/m^2}$ for upper and bottom surfaces, respectively. ε_0 is the permittivity of free space. The ratio

of ε_0 for surfaces to the permittivity for air is 4.5. Under static conditions, the relationship between the electric potential V and the electric field E is described by the following equation:

$$\vec{E} = -\vec{\nabla}V \tag{2}$$

The potential on the grounded border is set zero.

Table S1. The contact angle and roll-off angle of water droplet on the super-repellent surface (6 μl droplet for measurements), related to Figure 2.

Sample	Contact angle (°)	Roll-off angle (°)
Glass on stage	155±1	1±1
Glass suspended	155±1	1±1
Silicon suspended	155±1	1±1
Silicon on stage	155±1	1±1
Glass on stage after impact	155±1	3±2
Glass suspended after impact	142±2	43±8
Silicon suspended after impact	155±4	4±3
Silicon on stage after impact	155±4	4±3

Table S2. The characteristics of super-repellent surface substrate, related to Figure 4.

Materials	Dielectric constant (ε_r)	Thickness (mm)
PTFE	1.55	1
Glass	5.57	0.17, 0.5, 1
Si	12.1	0.3
ITO on glass	∞	0.0002

Table S3. Parameters for electrostatic simulations, related to Figure 5.

Dielectric	$\varepsilon_r = 1,\ w = 40$ mm, $\ l = 40$ mm
Charged surface	$\varepsilon_{r1} = 4.5,\ w_1 = 10$ mm, $\ l_1 = 0.17$ mm
Conductor plate	$\varepsilon_{r1} = 4.5,\ w_1 = 10$ mm, $\ l_1 = 0.17$ mm
Surface charge density P_{s1}	$-8\ \mu C/m^2$
Surface charge density P_{s2}	$8\ \mu C/m^2$
Distance between surfaces d	0.5 mm, 3 mm, 5 mm

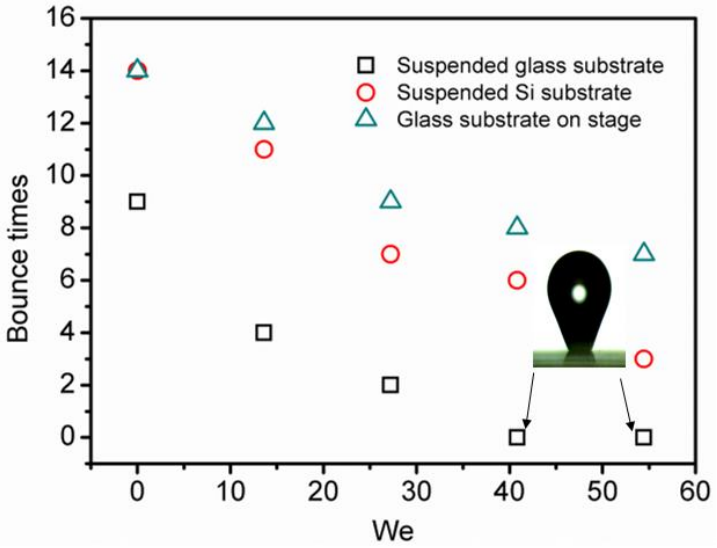

Figure S1. Droplet bounce times on charged super-repellent surface at different *We*, after releasing at the height of 1 cm, related to Figure 1. The bouncing times reduce with the increase of *We*.

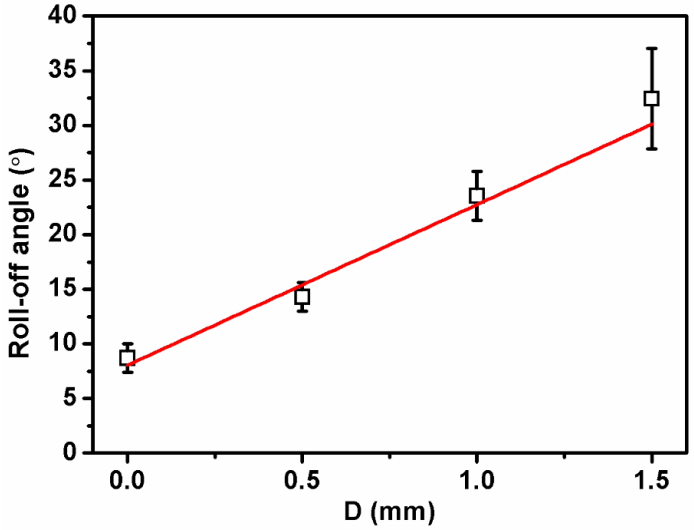

Figure S2. Roll-off angle as a function of electrostatic induction distance, related to Figure 5. The tested position is prior impact by water drop at *We* = 54.4.

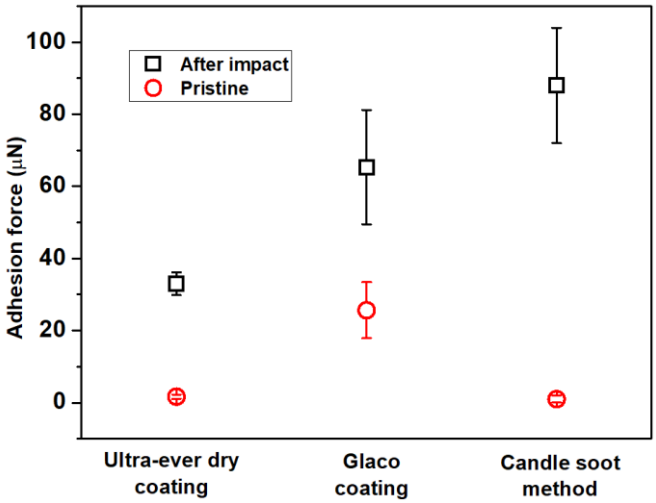

Figure S3. The adhesion of different types of super-repellent surfaces, related to Figure 5. The commercial coatings of Ultra-ever dry and Glaco are directly sprayed onto 170 μm-thick glass. These surfaces are impacted by a water drop at the *We* = 68.1.

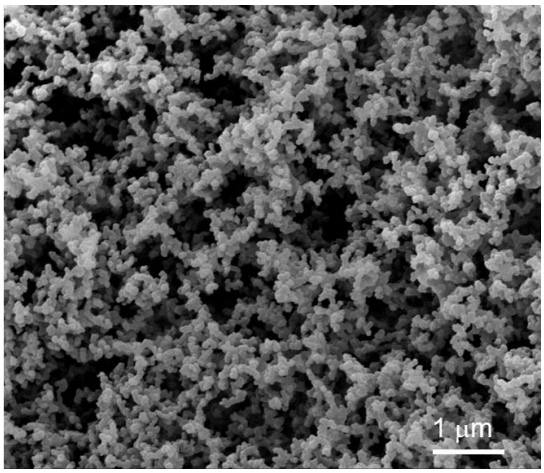

Figure S4. Morphology of the prepared super-repellent surface, related to Figure 3. The super-repellent surface consists of porous fractal structures.

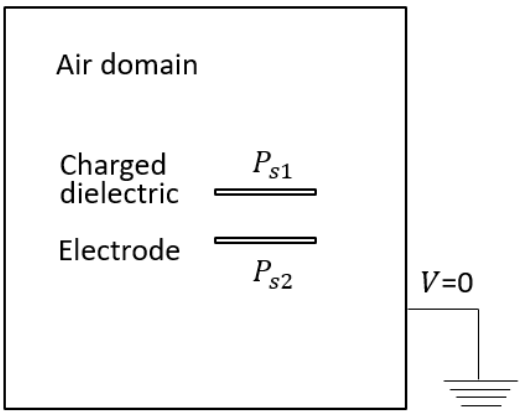

Figure S5. Geometry of electrostatic model in the simulation, related to Figure 5. The simulation region consists of two electrodes in an air domain, the boundary of which is ground connected.

SUPPLEMENTAL REFERENCES

Deng, X., Mammen, L., Butt, H.-J., and Vollmer, D. (2012). Candle soot as a template for a transparent robust superamphiphobic coating. Science *335*, 67-70.

Song, D., Song, B., Hu, H., Du, X., and Ma, Z. (2015). Contact angle and impinging process of droplets on partially grooved hydrophobic surfaces. Applied Thermal Engineering *85*, 356-364.